

A SURVEY OF SATELLITE GALAXIES AROUND NGC 4258

MEGHIN SPENCER^{1,2}, SARAH LOEBMAN^{1,3}, PETER YOACHIM⁴

Draft version August 8, 2021

ABSTRACT

We conduct a survey of satellite galaxies around the nearby spiral NGC 4258 by combining spectroscopic observations from the Apache Point Observatory 3.5-meter telescope with SDSS spectra. New spectroscopy is obtained for 15 galaxies. Of the 47 observed objects, we categorize 8 of them as probable satellites, 8 as possible satellites, and 17 as unlikely to be satellites. We do not speculate on the membership of the remaining 14 galaxies due to a lack of velocity and distance information. Radially integrating our best fit NFW profile for NGC 4258 yields a total mass of $1.8 \times 10^{12} M_{\odot}$ within 200 kpc. We find that the angular distribution of the satellites appears to be random, and not preferentially aligned with the disk of NGC 4258. In addition, many of the probable satellite galaxies have blue $u - r$ colors and appear to be star-forming irregulars in SDSS images; this stands in contrast to the low number of blue satellites in the Milky Way and M31 systems at comparable distances.

Subject headings: galaxies: kinematics and dynamics — galaxies: individual (NGC 4258) — galaxies: structure — galaxies: satellites

1. INTRODUCTION

The number, type and spatial distribution of satellite systems surrounding host galaxies can serve as a unique probe to theories of galaxy formation. In a Λ CDM universe, host galaxies such as the Milky Way (MW) are predicted to reside in vast dark matter halos. In this paradigm, the main galaxy is expected to be surrounded by numerous satellite dark matter halos that lie within a few 100 kpc of the central galaxy. It is reasonable to expect that many of these halos host luminous dwarf galaxies. Such satellite systems are potentially ideal dynamical tracers of the underlying mass distribution and can also probe the effect of environment on morphology, star formation, and quenching. Despite the theoretical utility of a well-sampled satellite system, most observations find only a handful of satellites per massive host outside the Local Group (LG).

A limiting factor in establishing robust samples of satellites beyond the LG is the inherent faintness of these objects. To circumvent this, some have taken a statistical approach, stacking large numbers of similar systems and inspecting aggregate properties (Prada et al. 2003; Zaritsky et al. 1993). However, stacking in this manner makes it impossible to study variation between systems, and thereby restricts the inferences that can be drawn. For example, recent observations of the MW and M31 satellite systems have found them to be preferentially aligned in extended disks (Kroupa et al. 2005; Conn et al. 2013; Ibata et al. 2013). Such results are impossible to replicate in studies that stack galaxies and requires detailed knowledge of particular isolated hosts with large numbers of satellites to verify the global significance.

In this light, one recent study (Kim et al. 2011, here-

after K11) focuses on the MW-like, barred spiral galaxy NGC 4258 (also known as M106) to identify a large sample of satellite galaxies. K11 use MegaCam on the Canada France Hawaii Telescope to observe a 1.7 by 2.0 degree field around NGC 4258 (roughly out to a projected radius of 130 kpc) and find 16 candidate satellite galaxies and 5 probable candidate satellite galaxies. These were selected based on the existence of literature radial velocities, resolvable stars, and/or extended and faint surface brightness structure. This catalog of 21 galaxies spans a wide range of morphologies, from dSph, dE, Sd, to Irr. Most of them have surface brightness profiles that are fit well by an exponential and have negligible color gradients. Additionally NGC 4258 satellites follow the Schechter luminosity function with a faint-end slope of $-1.19^{+0.03}_{-0.06}$, which is steeper than the LG slope (-1.06 ± 0.03) but flatter than the M81 slope ($-1.29^{+0.07}_{-0.03}$).

We revisit this work by spectroscopically observing a subset of the 16 satellite galaxies identified in the K11 sample to determine the prevalence of foreground/background galaxy contamination. We expand the K11 survey to include additional galaxies detected in the Sloan Digital Sky Survey (SDSS) that are also spatially near NGC 4258.

NGC 4258 is similar to the Milky Way in that it has a terminal rotational velocity of 208 km s^{-1} (Erickson et al. 1999), is a barred spiral galaxy, and has an average B-band surface brightness of 23.1 (Karachentsev et al. 2013).⁵ Due to its relatively nearby location (7.6 Mpc, Humphreys et al. 2013) and interesting inner disk morphology (resolved AGN and warped accretion disk, Caproni et al. 2007; Martin 2008), it has been the source of a wide array of galactic studies. Significantly, NGC 4258 possesses a water maser, which tightly constrains the distance to it with an error of only $\sim 3\%$ (Humphreys et al. 2008). Other distance measurements made with Cepheid variables and tip of the red giant branch (TRGB) magnitudes have reasonable agreement

¹ Department of Astronomy, University of Michigan, 500 Church Street, Ann Arbor, MI 48109

² Correspondence should be addressed to meghins@umich.edu

³ Michigan Society of Fellows

⁴ Department of Astronomy, University of Washington, Box 351580, Seattle, WA 98195

⁵ <http://www.sao.ru/lv/lvgdb/>

(Humphreys et al. 2013).

Aside from assessing the significance of foreground/background contamination in a photometrically derived satellite sample, we see three primary motivations to extend the K11 study of the NGC 4258 satellite system. One, using a Jeans equations based technique developed by Watkins et al. (2010), we can draw constraints on the total mass of NGC 4258. Two, we can assess if there is a preferential orientation for the satellites surrounding NGC 4258, as has been found for the MW (Kroupa et al. 2005), M31 (Conn et al. 2013; Ibata et al. 2013), and M81 (Chiboucas et al. 2013). Three, it has long been known that the color and morphology of MW and M31 satellites vary as a function of distance from respective hosts (see, for example, Mateo 2008). However, it has yet to be established if this apparent environmental effect holds outside the LG. Given its relative isolation from other massive perturbers and numerous candidate satellites, NGC 4258 provides an ideal testbed of the significance of proximity to the host galaxy to color and morphology of satellites.

For these reasons, we build upon K11’s work to assemble and leverage the most complete list of satellite galaxies surrounding a MW-like system outside the LG. The structure of this paper is as follows: Section 2 details our data collection/reduction process, including the target selection, observations, data processing, and velocity measurements. Section 3 provides a discussion of how we categorize the satellites and calculate the host mass. In the same section we present a discussion of the angular distribution and color range of the satellites. Section 4 contains concluding remarks.

2. DATA COLLECTION

2.1. Target Selection

We combine the K11 catalog of 16 potential satellites with additional candidates drawn from the SDSS database to produce a list of targets for spectroscopic followup. To select potential targets from SDSS, we searched within 2 degrees (projected radius ~ 250 kpc) of NGC 4258 and required that the r-band Petrosian radius be larger than $5''$ and the photometric redshift be less than 0.1. Minor color cuts were applied to ensure targets had galaxy-like colors. This list was sorted by r-band brightness, and then targets were manually inspected to remove any objects that were artifacts of SDSS such as shredded galaxies or bright star halos. Satellites were then ranked based on r-band magnitude, projected distance of the satellite away from the host, and photometric redshift, using the following formula: $\text{score} = \sqrt{\left(\frac{r}{r_{max}}\right)^2 + \left(\frac{d}{d_{max}}\right)^2 + \left(\frac{z}{z_{max}}\right)^2}$. The 30 highest scoring galaxies as well as the K11 satellites served as the basis for our observations. Due to limited observing time we did not obtain spectra for all of these objects. See Figure 1 for galaxy distribution in right ascension and declination relative to NGC 4258 and Table 1 for relevant properties from SDSS⁶ and NASA/IPAC Extragalactic Database (NED)⁷.

2.2. Observations and Data Reduction

We used five half-nights of observing time on the 3.5-meter Apache Point Observatory (APO) telescope with the Dual Imaging Spectrograph (DIS) to observe 29 targets. The wavelength was centered on 6799 Å for the red channel and 4502 Å for the blue, with each channel covering about ~ 1180 Å. The high resolution 1200 lines/mm grating was used with a slit width of $2''$. Observations were made in February, April, and May of 2011. Exposure times ranged from 5 to 20 minutes.

Ten bias frames were averaged and subtracted from all images. Nightly quartz lamp dome flats were normalized by a 9th, 10th or 11th order polynomial and divided out of the science images. Arc lamp Helium-Neon-Argon spectra were taken after slewing to a new target to correct for any small distortions in the mirror and instrument while the telescope was in motion. Arc lamp frames were used to wavelength calibrate the corresponding science spectra. Standard star observations taken at the beginning and/or end of each night. These flux standards were used to eliminate the instrument response signature in the spectra. Typical seeing was $1.6''$, and the standards were observed at low airmass. The background was subtracted by using regions off-target but along the slit.

Spectra were corrected to the heliocentric rest frame and were combined when repeat observations were made on the same night. Spectra from the red and blue channels were reduced with the same method. Completely reduced spectra have a scale of 0.58 Å/pixel for the red channel and span a wavelength range of ~ 6210 to 7390 Å; the scale for the blue channel is $.61$ Å/pixel, spanning a range of ~ 3870 to 5130 Å. See Figure 2 for a sample of reduced spectra.

Objects observed with APO are listed in Table 1 along with the J2000 right ascension, declination, SDSS r-band magnitude, measured heliocentric radial velocity, and literature distances. Galaxies will hereafter be referred to by last three (or four) digits of their SDSS DR7 object ID. For a full SDSS ID refer to Table 1.

2.3. Velocity Measures

Depending on the size of the target galaxy, we extract between 1 and 20 spectra along the spatial dimension. For each extracted spectrum, we use Penalized Pixel-Fitting (pPXF) (Cappellari & Emsellem 2004) and Gas AND Absorption Line Fitting (GANDALF) (Sarzi et al. 2006) algorithms to fit stellar velocities and emission line velocities in both the red and blue spectra. For stellar templates, we use the single stellar population galaxy models from Vazdekis et al. (2010). For galaxies that were spatially extended, we fit rotation curves to the measured velocities to find the dynamical centers of the systems and systemic velocities.

The red emission lines ($H\alpha$, [SII]) are usually the brightest features. The red spectra are also better calibrated since we only have ~ 5 arc-lines in the blue. We therefore adopt the red emission line velocity, or if it is not available, the blue stellar velocity as the systematic velocities of our galaxies.

Since many of these galaxies are spatially extended, we expect the primary source of error to be due to imperfect placement of the spectrograph slit. Given the high signal in most of our spectra, we expect velocity errors of order

⁶ <http://sdss3.org>

⁷ <http://ned.ipac.caltech.edu/>

10 km s⁻¹. Formally, the errors could be smaller, but we expect systematic errors (slit-placement, kinematic vs photometric center, etc.) will limit us as well. We assume the maximum in the stellar continuum corresponds to the dynamical center of each galaxy.

Our velocities agree with the available SDSS values within the root mean square scatter of 10 km s⁻¹ in all but three cases. Two of the galaxies (SDSS IDs 911 and 621) have bright off-center star forming regions which were targeted by SDSS. The last galaxy (782) remains discrepant; despite being a relatively bright object, none of the measurements (ours, SDSS, or NED) agree particularly well.

Our velocity for NGC 4258 also agrees with literature values. To derive this, we carefully extracted the spectrum from a small central region, as NGC 4258 has a very sharply rising rotation curve which can skew the result if the extraction is not symmetric.

3. ANALYSIS

Below we present three findings that were made with the combined SDSS and APO data. The first section describes how we categorize galaxies as probable and possible satellites versus background galaxies. The second section explains our mass calculation of NGC 4258. The third section examines the angular distribution of satellites, and the fourth section discusses the color of our satellite galaxies.

From this point forward, any mention of a velocity refers to the velocity relative to NGC 4258. The relative velocity is defined as the line of sight velocity of that galaxy minus the line of sight velocity of NGC 4258. A histogram of all these relative velocities is shown in Figure 3 as a red line. It is immediately apparent from this figure that there are many more galaxies that are redshifted with respect to NGC 4258 than blueshifted. By symmetry, we expect a similar number of true satellite galaxies to be redshifted as blueshifted (Zaritsky 1992). In addition there is a peak around 300 km s⁻¹ indicating that there might be some other structure just beyond NGC 4258. For these reasons, we conclude that there is significant contamination from background galaxies in our sample. Before we can perform any analysis on our sample of galaxies or on the host itself, we must discard non-members.

3.1. Separating Satellites from Background Galaxies

In order for a dwarf to be considered a satellite it must be bound to the host galaxy. That is, it must have a total velocity less than the escape velocity of the system *and* have a distance similar to that of the host (Zaritsky et al. 1993). To determine which of our dwarf galaxies could satisfy the first requirement, we plot the line of sight velocity with respect to the host against the projected radius (Figure 4).

Next, we calculate the escape velocity as a function of radius for three different mass distributions: a point mass, an NFW profile (Navarro et al. 1996), and a Burkert profile (Burkert 1995). Disk components are included for the latter two profiles.

The NFW profile is described by

$$\rho_{NFW} = \rho_H \frac{1}{x(1+x)^2}, \quad (1)$$

and the Burkert profile is described by

$$\rho_{Bur} = \rho_H \frac{1}{(1+x)(1+x^2)} \quad (2)$$

where ρ_H is density scale, $x = R/R_H$ and R_H is the core radius for an NFW profile, which is of the order 10 kpc. We iterate on ρ_H and R_H in our analysis. The disk surface density that we employ is

$$\sigma_D = \frac{M_D}{2\pi R_D^2} e^{-r/R_D} \quad (3)$$

where the mass of the disk, M_D , is $6 \times 10^{10} M_\odot$ and the scale radius of the disk, R_D , is 2.6 kpc. Importantly, since we only know 1-D velocities (radial velocities) of our galaxies, we assume they obey velocity isotropy⁸. In this limit, we can compare our line of sight velocities with the escape velocities predicted for each profile by dividing the profiles by $\sqrt{3}$. We have over plotted $\pm(V_{esc}/\sqrt{3})$ for the three profiles in Figure 4.

Next, we determine the best fit parameters to these profiles. As a first guess we use the parameters for the Milky Way as defined by Nesti & Salucci (2013). Because the NFW and Burkert models yield nearly identical results, we opt to use the NFW profile for further analysis rather than both models. To further refine the density models we need to know additional information about the system. If there was a selection of galaxies with reliable distance measurements that match NGC 4258 and have velocities within a reasonable range, we can conclude that such galaxies must be bound to the system and leverage them to constrain the halo parameters. This is the case for two of our 47 galaxies (996 and 207), which have tip of the red giant branch (TRGB) distances within the errors of the distance to NGC 4258 (Munshi & Macri 2007; Karachentsev et al. 2013). More importantly, they are located near the edge of the NFW escape velocity profile and can be used to create lower limit boundaries for the profile. We increase ρ_H and R_H so that these two satellites fall within the NFW escape velocity profile. Thus we assume density and radius values for the NFW model of $\rho_H = 1.4 \times 10^7 M_\odot/\text{kpc}^3$ and $R_H = 16$ kpc.

We now use our best-fit lower limit NFW profile to determine further satellite membership. Any galaxy that has a line of sight velocity that falls within the NFW $\pm(V_{esc}/\sqrt{3})$ lines in Figure 4 is a strong candidate for being a satellite galaxy (but see Barber et al. 2013, for possible confusion at large projected radii). Eight galaxies fall within the $\pm(V_{esc}/\sqrt{3})$ boundaries and have projected radii of less than 200 kpc; they are deemed the most probable satellites, and are tagged with a ‘‘Y’’ for Yes in our catalog. Galaxies that fall within the $\pm(V_{esc}/\sqrt{3})$ boundaries but have projected radii of greater than 200 kpc, are tagged with a ‘‘M’’ for Maybe.

Next we relax our initial assumption about velocity isotropy and consider the case when most of the total velocity is along the line of sight⁹; a system is bound in this scenario if the line of sight velocity is simply less

⁸ That is, $\sim V_x = V_y = V_z$; it then follows that the 3-D velocity of a satellite is $|V_{tot}| = \sqrt{3V_x^2}$.

⁹ In this case, $|V_{tot}| \sim V_x$

than the total escape velocity. This is a possible but not probable scenario. Hence, we categorize galaxies with a line of sight velocity greater than $\pm(V_{esc}/\sqrt{3})$ but less than $\pm V_{esc}$ as possible satellites, and tag them with an “M” for Maybe as well.

17 galaxies fall beyond the total escape velocity profile. We categorize them as non-members, and tag them in our catalog with an “N” for No. The remaining 14 galaxies lack velocity information. At this time, we draw no conclusion about their membership. These galaxies are indicated in Table 1 with an “X” for eXcluded. They are not included in our subsequent analysis but would be strong candidates for further follow-up.

We consider the steps outlined above a good first pass at determining membership. However, distance estimates to these objects can help us refine our individual classifications. The literature contains distance measurements for 13 of our 47 galaxies. Here we amend a few of our previous Y/M/N/X categorizations on the basis of these values, as outlined below.

Recall NGC 4258 is 7.6 Mpc away. Galaxy 850 was initially classified as “M;” however, its average distance in NED is 15.7 Mpc from Tully Fisher and surface brightness fluctuation measurements; due to the large separation in distance, it is reclassified as a “N” for background galaxy. Galaxies 909, 042, and 206 have average Tully Fisher distances in NED of 17.9, 14.4, and 21.05 Mpc respectively; again, they are reclassified as “N.” Another galaxy we reclassify is 782, which has a single Tully Fisher distance in NED of 21.2 Mpc; we demoted from “Y” to “N.” Finally, galaxy 911 has a TRGB distance of 5.63 Mpc in NED. It was originally a “Y” but is demoted to “N” as it is a foreground galaxy. Any galaxies unmentioned retain the same membership classifications as before. These final classifications are listed in Table 1.

We add one additional galaxy to our list from archival HST data analyzed by L. Macri and F. Munshi (see, Munshi & Macri 2007). They present the TRGB distance to galaxy 358. We categorize it as an “M” galaxy since the distance is similar to the host galaxy, but refrain from a higher ranking because we do not have a velocity measurement. Additionally, Macri and Mushi also provide a TRGB distance for 207 that is consistent with NGC 4258.

It should be noted that seven of the galaxies we considered (067, 207, 4639, 422, 970, 678, 012) are listed with distances of 7.8 Mpc in Karachentsev et al. (2013) based upon K11’s photometric work. 7.8 Mpc is the distance to NGC 4258 found from Cepheid measurements of Newman et al. (2001). We do not list these distances in Table 1 because, as we demonstrate here, membership based on photometry alone is uncertain.

When taking into consideration the available velocities and distances, we conclude that 4 of the objects classified by K11 are probable satellites (072, 207, 277, 996), 2 are possible satellites (593, 634), 3 are not satellites (782, 850, 909), and 7 are still uncertain (012, 067, 422, 678, 828, 970, 4639). We note that 072, also known as NGC 4248, has long been considered a satellite galaxy (van Albada 1977). See Table 1 for mapping between K11 ID and SDSS ID, as well as Figure 1.

We conclude that 8 of the galaxies we consider have the highest probability of being satellites. This repre-

sents 17% of our sample. A dwarf galaxy survey done by Carrasco et al. (2006) found only 78 out of their 409 target galaxies within four clusters were actually members, equating to a 19% yield. Since the surface density of galaxy clusters is much larger than that of field galaxies, we consider the results of the Carrasco et al. (2006) survey as an upper limit for how well we expect to be able to select system members. However, we caution that without knowing both velocities and distances, it is impossible to state with absolute certainty whether a galaxy is a satellite, and it is still quite possible that some of our most probable sample are in fact non-members.

To summarize, we adopt the following classification scheme:

- Probable Satellites (“Y”): galaxies with distance measurements consistent with NGC 4258 or no known distances; line of sight velocity within $\pm(V_{esc}/\sqrt{3})$ and have projected radii less than 200 kpc.
- Possible Satellites (“M”): galaxies with distance measurements consistent with NGC 4258 or no known distances; line of sight velocity greater than $\pm(V_{esc}/\sqrt{3})$ but smaller than $\pm V_{esc}$, or line of sight velocity within $\pm(V_{esc}/\sqrt{3})$ but with projected radii greater than or equal to 200 kpc but less than 300 kpc.
- Unknown if Satellites (“X”): galaxies with distance measurements consistent with NGC 4258 or no known distances; galaxies with no known line of sight velocities; projected radii less than 300 kpc.
- Not Satellites (“N”): galaxies with distance measurements inconsistent with NGC 4258 or velocities outside $\pm V_{esc}$.

Based upon on these criteria, we categorize 8 objects as probable satellite galaxies, 8 as possible satellite galaxies, and 17 as non-members; for 14 galaxies we draw no conclusion.

3.2. Halo Mass

With this collection of probable satellite galaxies, we next aim to estimate the dynamical mass of NGC 4258. Watkins et al. (2010) publishes a set of robust mass estimators for cases where only the projected radius and line of sight velocity of each target are known (as opposed to true radii and peculiar velocities). They assume the population of satellites is spherically symmetric. The relevant equations are:

$$M = \frac{C}{G} < v_{\text{los}}^2 R^2 >, C = \frac{(\alpha + \gamma - 2\beta)}{I_{\alpha,\beta}} r^{1-\alpha} \quad (4)$$

$$I_{\alpha,\beta} = \frac{\pi^{1/2} \Gamma(\frac{\alpha}{2} + 1)}{4\Gamma(\frac{\alpha}{2} + \frac{5}{2})} [\alpha + 3 - \beta(\alpha + 2)]. \quad (5)$$

where M is the galaxy mass, G is the gravitational constant, α is a fiducial radius at which the power-law approximation for the relative potential is valid, β is the Binney anisotropy parameter that depends on the tangential and radial velocity dispersions, γ is the power law index of the radial density distribution of satellites, r_{out}

is the upper limit of a gravitational field that is scale-free, and $\Gamma(x)$ is the gamma function, where $\Gamma(x) = (x - 1)!$. We use $\alpha = 0$ (satellites move in a large-scale mass distribution with a flat rotation curve), $\beta = 0$ (isotropic satellite orbits), and $\gamma = 2$ (the satellite density falls off as r^{-2}).

Incorporating our 8 probable satellite galaxies into the mass calculation, we find the mass of the host to be $3.1 \pm 0.7 \times 10^{12} M_{\odot}$ out to a radius of 200 kpc. Including the 8 probable satellites plus the 3 possible satellites that fall within $\pm(V_{esc}\sqrt{3})$ but have projected radii greater than 200 kpc, we find the mass of the host to be $3.7 \pm 1.0 \times 10^{12} M_{\odot}$ out to 240 kpc. Current estimates for the MW range between $0.6 \times 10^{12} M_{\odot}$ and $3.1 \times 10^{12} M_{\odot}$ within the virial radius (McMillan 2011; Boylan-Kolchin et al. 2013; Barber et al. 2013).

An alternative way of calculating the mass is by integrating the NFW density profile over an appropriate range of radius. Utilizing the NFW profile derived in Section 3.1, we determine the total mass out to 200 kpc is $1.8 \times 10^{12} M_{\odot}$. Any uncertainty here is due to the fact that we have 1-D velocities and projected radii.

3.3. Satellite Distribution

Several studies of the MW, M31, and M81 have found that satellites exist in a plane centered around the host (Kroupa et al. 2005; Conn et al. 2013; Ibata et al. 2013; Chiboucas et al. 2013). K11 find their sample of 16 satellites are preferentially aligned along the disk of NGC 4258. We reassess these findings based on our revised satellite list.

A rigorous evaluation would consider both a satellite's angle and projected distance away from the disk before drawing conclusions about the angular dependence. However, the disk of NGC 4258 is highly inclined relative to our line of sight; this minimizes the impact of projection effects, which could cause a satellite elevated above the disk to instead appear aligned with the disk. Because of this we only consider the angular separation between a satellite and the disk plane. We use a position angle of 150° (de Vaucouleurs et al. 1991).

Figure 6 displays the cumulative angular distribution of three subsets of satellites. The blue solid line traces the probable satellites; the dashed green line traces the probable plus possible satellites; and the red dash-dotted line traces the original K11 satellites. Data has been folded from 360 degrees to 90 degrees to allow for better statistical sampling. An angle of 0 degrees indicates a satellite galaxy is perfectly aligned with the disk of the host (i.e. major axis alignment); an angle of 90 indicates a galaxy is not at all aligned with the disk and might instead be aligned with the minor axis of the host. In Figure 6, a black dash-dotted line marks the case where there is no angular dependence, that is, there are just as many satellites at low angles as high angles. Distributions that grow faster than this line are said to be preferentially aligned with the disk; distributions that grow slower than this line are not aligned with the disk.

Overplotted on Figure 6 are the one sigma envelopes for random distributions drawn from samples of eight and 16 satellites, shown in blue and red respectively. Our probable sample has 8 satellites; the probable plus possible sample and the K11 sample both have 16 satellites.

All three distributions grow faster than the random distribution; however both the probable and probable plus possible samples fall (marginally) within the envelopes of what is allowed by a random distribution.

For completeness, we have used the IDL routine *ksone* to run a one-sample Komolgorov-Smirnov (KS) test on the data to quantitatively assess if the angular distributions of probable satellites, possible plus probable satellites, and K11 satellites are drawn from a random distribution. However, we caution that the KS test requires a relatively large number of data points to properly reject the null hypothesis (that the sample is drawn from a random uniform distribution).

The KS statistic (D) specifies the maximum deviation between the data and a supplied distribution; D varies between 0 and 1. Larger D values indicate that the data and supplied distribution are significantly different. The significance level (p -value) of the KS statistic is also considered; the p -value is the probability of drawing from a random distribution and obtaining results as extreme or more extreme than the data. P -values vary from 0 to 1; a large p -value indicates that it is highly likely that one will generate samples like the data.

We make two comparisons to a flat distribution, where a satellite is equally likely to be at any angular position: we consider our catalogs of probable satellites, and probable plus possible satellites. The KS statistics for these are $D=0.24$ and 0.18 with significance levels of $p=0.66$ and 0.63 respectively. Since the D numbers are small and p -values are large, this means with a high confidence level, our samples of probable and probable plus possible satellites are drawn from a flat distribution.

Ever since Holmberg initially found satellite galaxies are preferentially aligned along the minor axis of their host (Holmberg 1969), there have been a steady stream of conflicting results regarding satellite galaxy alignments (see Bailin et al. 2007, and references therein). Besides numerous observational disagreements, there is also no broad theoretical agreement on whether satellites should be aligned at all or found on randomly oriented orbits (Zentner et al. 2005; Kroupa et al. 2005). There are two standard interpretations of satellites existing in a disk; either they recently merged as an infalling group, or they tend to fall along cold dark matter filaments (Hartwick 2000). On the other hand, a lack of any orientation could imply that the host galaxy has not accreted any new dwarfs in recent cosmic times. While our findings very loosely support the latter hypothesis, we feel that we have too few satellites to draw definitive conclusions. There may even be an alternative interpretation when taking satellite colors into consideration (see Section 3.4).

3.4. Satellite Morphology

Figures 7 and 8 display the SDSS images of our probable and possible satellites respectively. From these images, is immediately apparent that the vast majority of these satellites are blue irregulars. We plot further in Figure 9 a map of the Sloan $u - r$ colors of the satellites as they appear on the sky. Colors less than 2.2 are blue, late-type galaxies. All but two of our probable satellites have $u - r$ colors less than 1.7. The remaining two have colors less than 2.15. Adding to that, all of the possible satellite galaxies have $u - r$ colors less than 1.6. Given our technique for identifying the line of sight velocity of

these galaxies, this is not surprising (that is, our catalog is not complete, as the method is biased against red, dim satellites). What is surprising is the sheer number of blue satellites; if this system was like the MW or M31, we would expect many fewer blue star forming satellites at small projected radii.

To further stress this point, we replicate a color-magnitude plot from Mateo (1998) shown in Figure 10. Color transformations from Chonis & Gaskell (2008) are used to move from *g* and *r* to *B* and *V*. Galaxies that fall below the black line are blue late-type galaxies; galaxies above the black line are red early-type galaxies. Many of our probable and possible galaxies that have small projected radii are found below the line.

It is conventionally thought that galaxies experience quenching as they fall inward toward the host (see, for example, Geha et al. 2012). Since our satellites are blue star-formers they most likely have not had enough time to be quenched. As mentioned in the previous section, this might imply that they have recently been accreted to the system.

Again, we are not making an argument for completeness here because we are only sensitive to the brightest satellites and therefore miss dimmer dwarf spheroidals. However, even in an incomplete sample we find a large number of blue, late-type galaxies. Our results are consistent with the photometric work of Ludwig et al. (2012) for NGC 7331.

4. DISCUSSION AND CONCLUSION

4.1. *Necessity of Spectroscopy*

As we have demonstrated, satellite membership is challenging to determine. It cannot be done from photometry alone, nor spectroscopy alone, but instead requires, at minimum, a combination of the two. With photometry, one can make a good first guess as to which galaxies might be satellites based on resolvability of stars and surface brightness as was done by K11. Spectroscopy can help narrow that sample, as we have shown here. To further refine the selection, distance measurements are needed. Finally, to verify a galaxy as a satellite with absolute certainty would require orbital radius and proper motions. Without these, it is impossible to confidently declare satellite membership.

While our sample of satellites does take velocities and distances into consideration, we caution that it might still contain non-members in the foreground and background. Since small number statistics are in play for these sorts of systems, it only takes a couple non-member galaxies to produce misleading conclusions about the characteristics of the sample as a whole. This is why we choose four categorizations for our satellites: probable, possible, non-member, and unknown. We do not refer to any of the satellites as confirmed.

Despite our cautionary language, we cannot emphasize enough that our sample has much better constraints than a purely photometrically derived ground-based satellite catalog. That is, while it is not complete and perhaps suffers some minimal degree of contamination, it is certainly the most reliable catalog of NGC 4258 satellites to date.

4.2. *Conclusion*

We present a spectroscopic catalog of 47 dwarf galaxies surrounding NGC 4258. Fifteen of these targets did not previously have published redshifts. A histogram of line of sight velocities of potential satellite galaxies indicates that a substantial fraction are background galaxies; without proper motions (or realistically, distances to the galaxies) there is no easy way to determine which are bound to NGC 4258 and which are background contaminants. Using an NFW profile to eliminate any obvious interlopers, we classify 8 of our dwarf galaxies as probable satellites and 8 as possible satellites. Our selection criteria are based upon distance measurements and velocities. With this sample of satellite galaxies, we make four conclusions:

(1) The mass yielded when using the 8 probable satellite galaxies in a mass estimator based on the spherical Jeans equation is $3.1 \pm 0.7 \times 10^{12} M_{\odot}$ out to a radius of 200 kpc. If we instead integrate our NFW profile, we find the mass to be $1.8 \times 10^{12} M_{\odot}$ out to 200 kpc.

(2) The orientation of the probable and possible plus probable galaxy subsets do not indicate a strong preferential alignment with the disk.

(3) A large number of the probable satellites are blue irregulars, which is atypical in comparison to the MW and M31 systems.

(4) Satellite membership is difficult to identify when only photometry is utilized. We conclude that velocity and distance measures are necessary to determine satellite membership with any certainty.

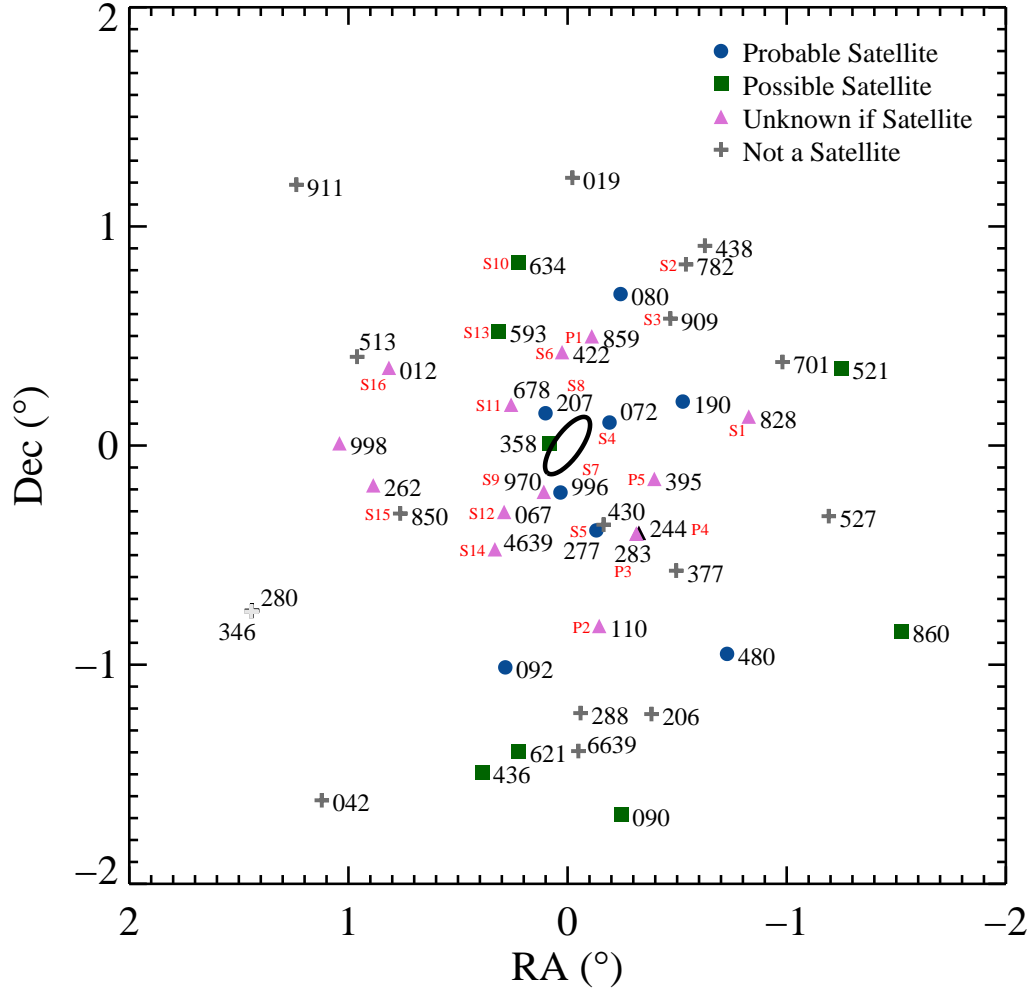


Figure 1. Locations of the considered galaxies on the sky. North is up; east is left. A large central oval represents the location, inclination, and size of NGC 4258. Each galaxy is labeled with the last three or four digits of its SDSS ID that uniquely identify it, and the K11 ID when available. Various plot symbols represent the membership categorizations that we make in Section 3.1. Blue circles are probable satellites (classified as “Y”); green squares are possible satellites (classified as “M”); gray pluses are background galaxies (classified as “N”); pink triangles are galaxies that lack velocity information (classified as “X”).

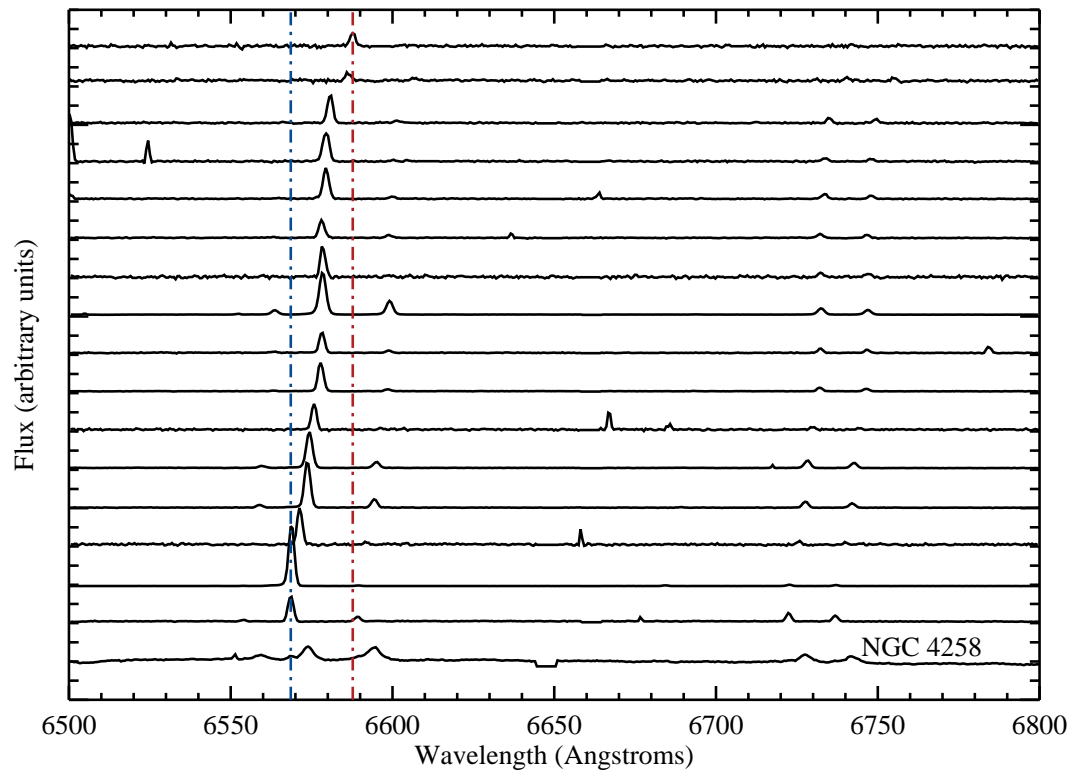


Figure 2. Spectra for 16 of the observed galaxies that have redshifts similar to that of NGC 4258. Spectra shown are from the red channel of DIS. The spectrum of the host galaxy is shown at the bottom. H α is the large emission line on the left and is bracketed by the [NII] doublet. On the right is the [SII] doublet. These five emission lines were used to determine redshifts of the galaxies. Vertical red and blue dashed lines mark the location of H α for the highest and lowest redshifted satellites respectively.

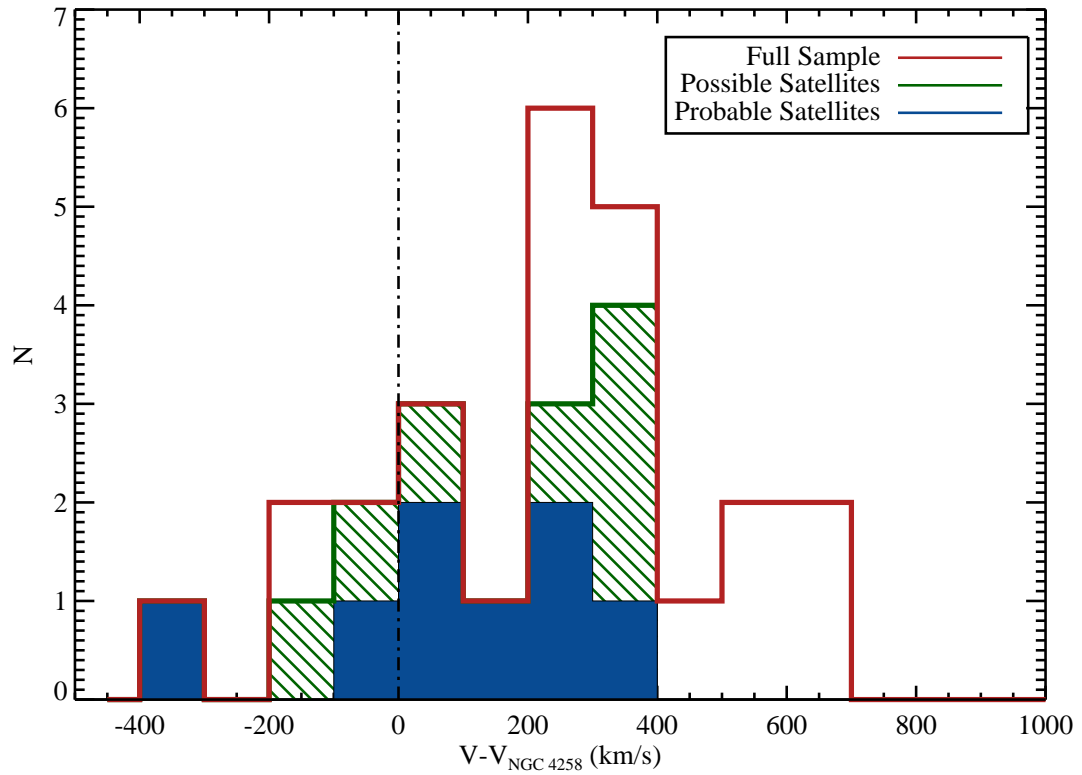


Figure 3. Histogram of the number of satellites in each 100 km s^{-1} velocity bin. The vertical black line marks the systemic velocity of NGC 4258. Notably, more galaxies are redshifted with respect to NGC 4258 than blueshifted, indicating the presence of background galaxies (Zaritsky 1992). In Section 3.1 we discuss how we narrow down the sample to probable satellites (blue filled region) and possible satellites (green filled region). The entire sample of galaxies is outlined in red. See Figure 4 for how these satellites are classified.

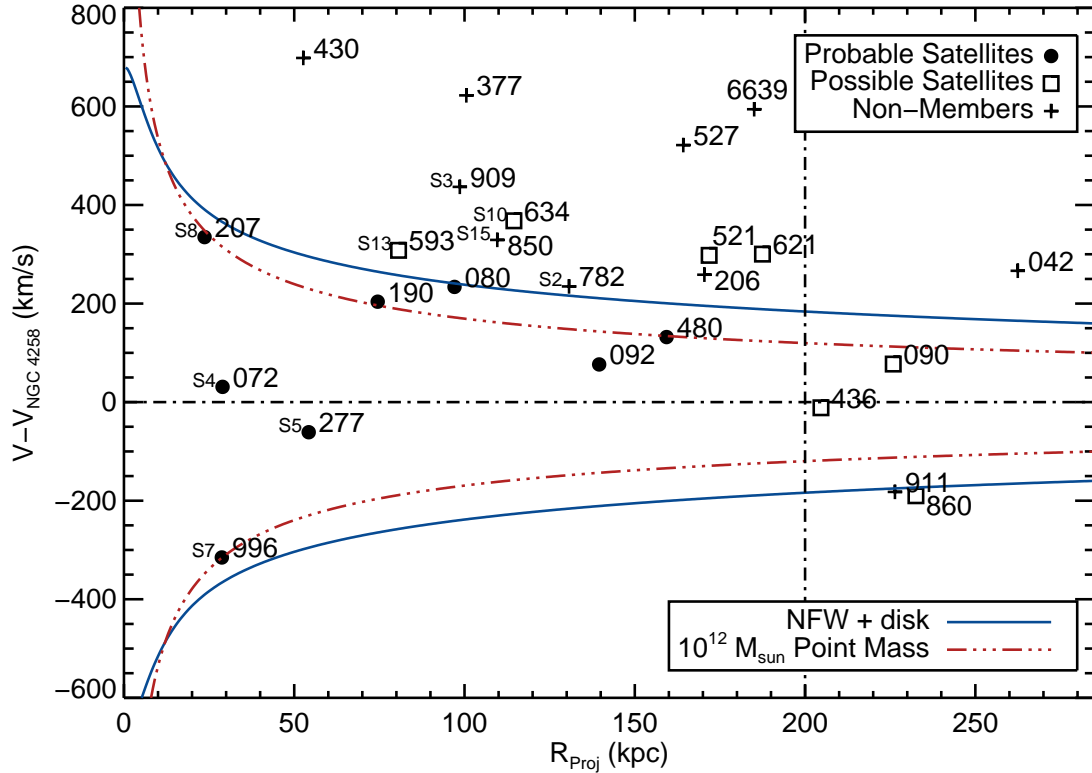


Figure 4. Projected radius vs line of sight velocity with respect to NGC 4258. Potential satellite galaxies are marked and labeled with the last three or four digits of their SDSS ID and K11 ID when relevant. Filled circles are objects classified as probable satellites; open squares are possible satellites; pluses are non-members. Blue and red lines trace the escape velocity from a disk+NFW profile and $1 \times 10^{12} M_{\odot}$ point mass. Escape velocity profiles are divided by $\sqrt{3}$ as we assume velocity isotropy in order to compare with the observed galaxy radial velocities. Objects beyond 200 kpc (vertical black dashed line) are at best listed as possible rather than probable satellites given their large projected radius (Barber et al. 2013).

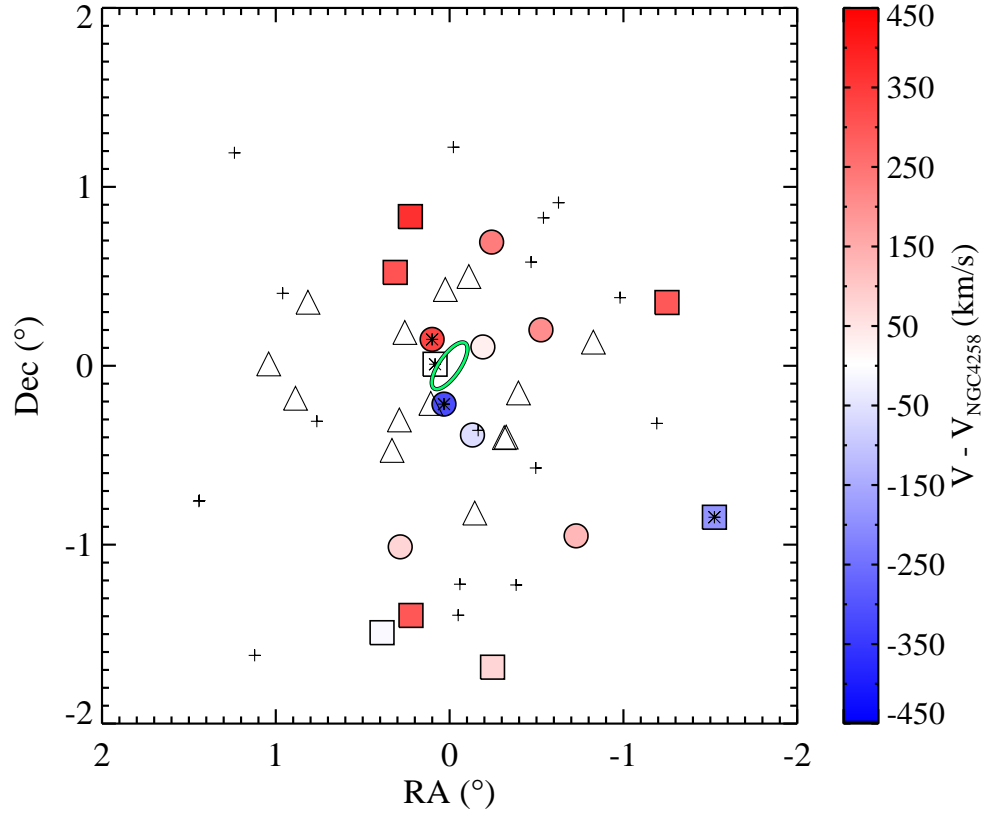


Figure 5. Line of sight velocity for each satellite as it appears in the sky. Red indicates the satellite is redshifted with respect to the host; blue indicates the satellite is blueshifted with respect to the host. The green ellipse marks the size, location, and inclination of NGC 4258. Circles are probable satellites (classified as “Y”); squares are possible satellites (classified as “M”); pluses are background galaxies (classified as “N”); triangles are galaxies that lack velocity information (classified as “X”). The asterisks mark galaxies with TRGB distances; the two circles with asterisks are the galaxies we used to select NFW parameters.

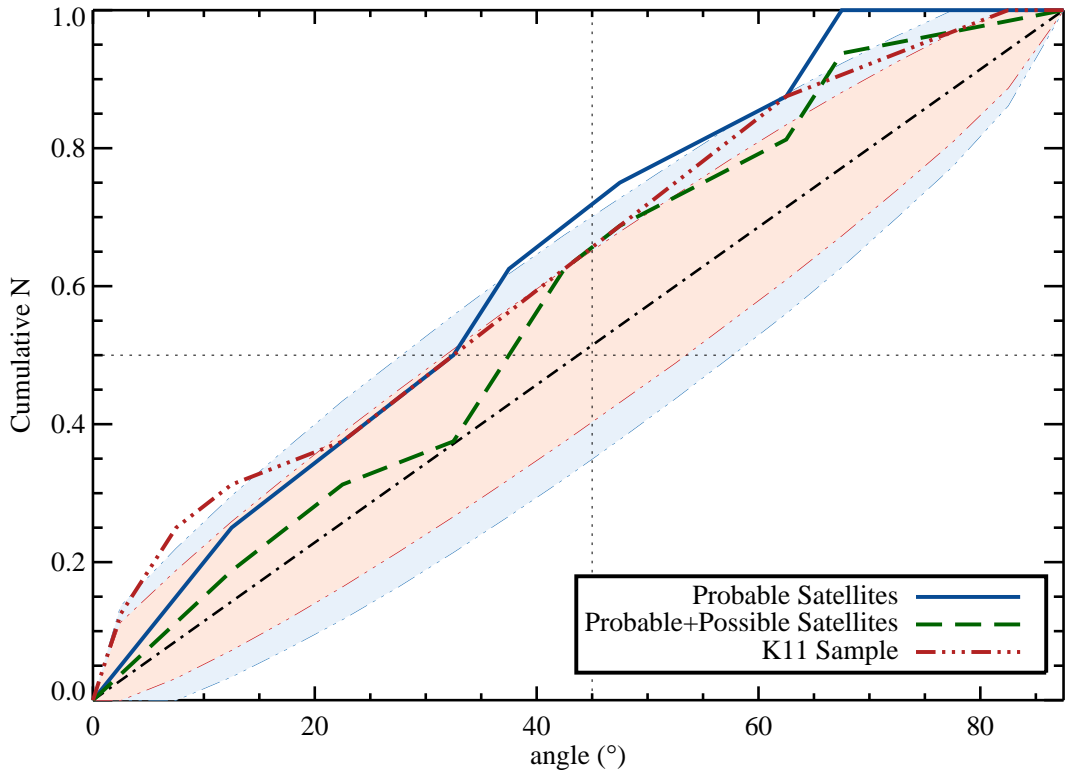


Figure 6. Cumulative histogram showing angle between each satellite and the host’s disk. The solid blue line indicates the 8 probable (“Y”) satellite galaxies found in this study; the dashed green line indicates the 8 probable plus 8 possible satellite galaxies (“Y” + “M”); and the dash-dotted red line indicates the 16 satellite galaxies from K11. The blue and red shaded regions are the one sigma envelopes for random distributions drawn from samples of 8 or 16 satellites respectively. The blue and green samples of satellites are consistent with there being no angular dependence around the disk of NGC 4258, shown as a straight black dash-dotted line along the center of the shaded region.

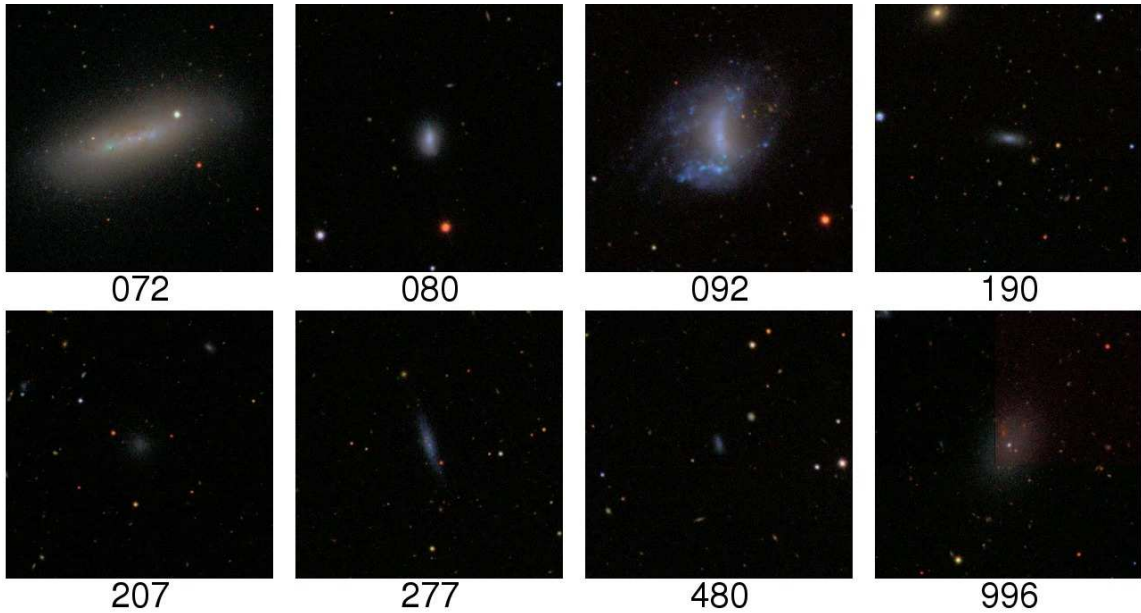


Figure 7. SDSS images of probable (“Y”) satellites. The last three digits of each SDSS ID are listed below the respective image. The images are scaled to be 3.38 arcmin in diameter.

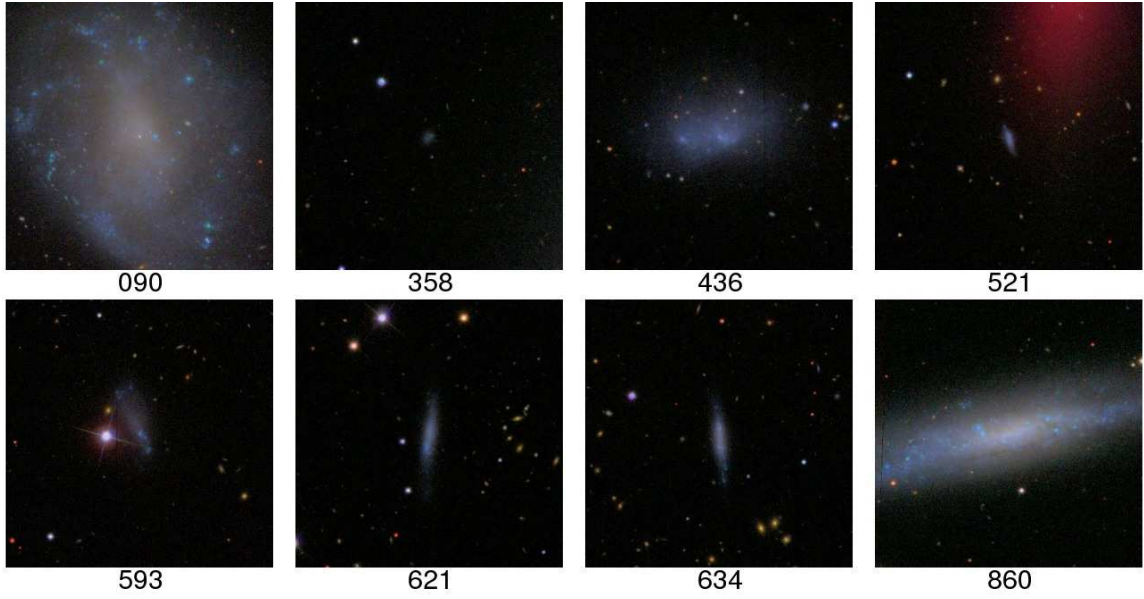


Figure 8. SDSS images of possible (“M”) satellites. The last three digits of each SDSS ID are listed below the respective image. The images are scaled to be 3.38 arcmin in diameter.

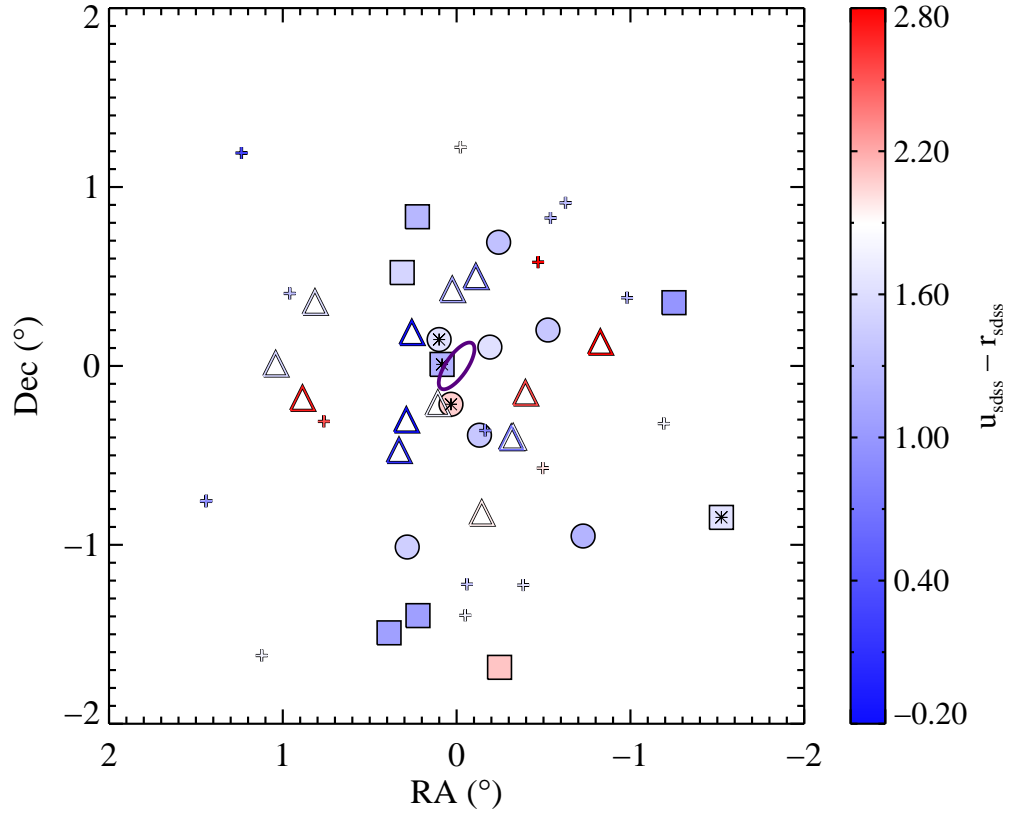


Figure 9. SDSS $u-r$ colors for satellites as seen on the sky. Red colored symbols represent redder galaxies; blue colored symbols represent bluer galaxies. Symbol shapes are the same as in Figure 5. Most of the probable (“Y”) satellites are bluer. This is in contrast to the MW/M31 satellite system.

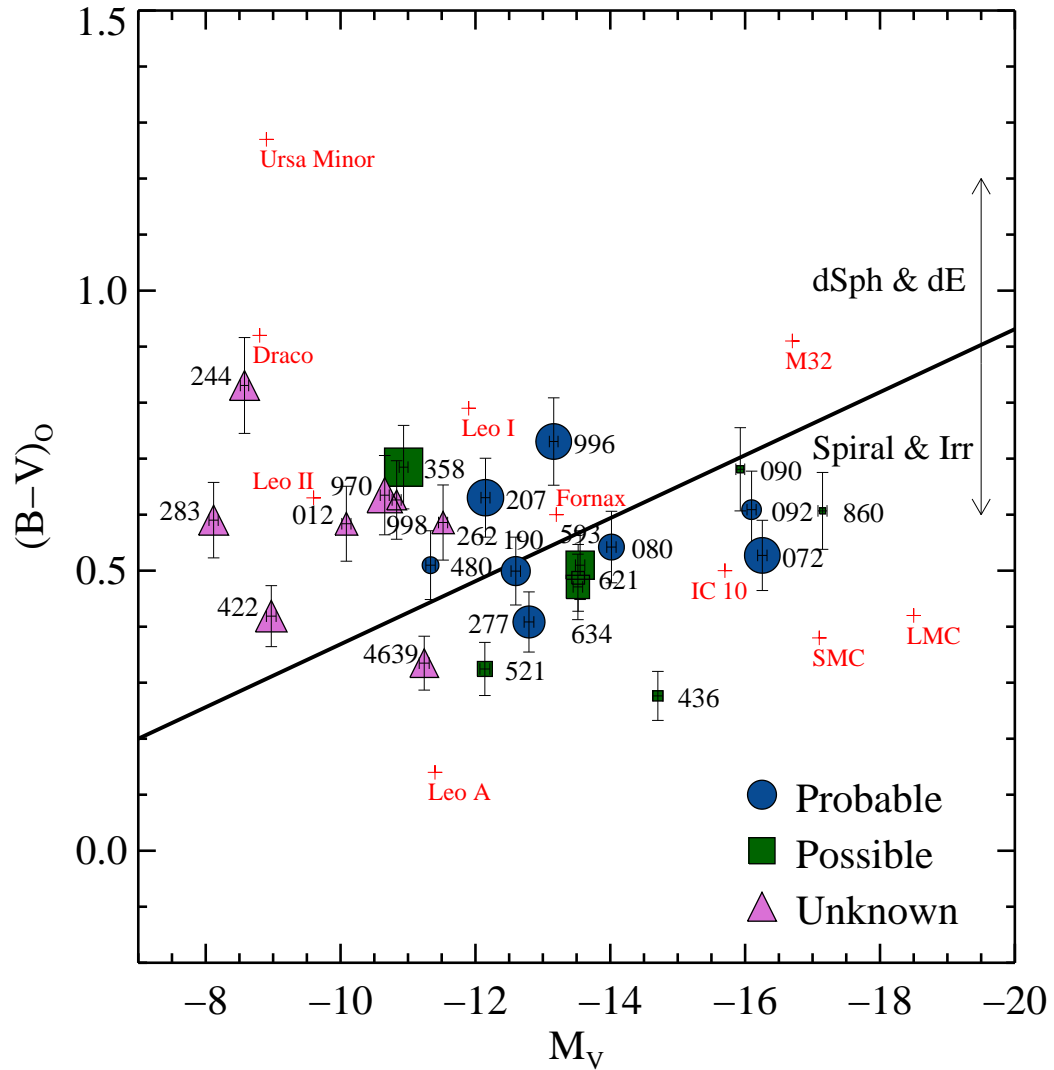


Figure 10. Extinction corrected B-V colors of the galaxies plotted against absolute V-band magnitude. Blue circles are probable (“Y”) satellites, green squares are possible (“M”) satellites, and pink triangles are galaxies that lack velocity information (“X”). Symbol size indicates projected radius; large symbols are satellites with a small projected radius; small symbols are satellites with a large projected radius. Several LG dwarf galaxies are shown as red pluses. Galaxies below the line are said to be blue; galaxies above the line are said to be red.

Table 1

Summary of galaxy properties from our observations and the literature. All velocities are relative to the heliocentric radial velocity. Column 3 is the ID given by K11; entries of N/A in the APO velocity column are galaxies that we observed but could not extract a radial velocity for; entries of “>10,000” are galaxies that we observed that were high redshift; the Status column is the member categorization that we describe in Section 3.1. “Y” is a probable satellite; “M” is a possible satellite; “N” is not a satellite; “X” is a galaxy lacking velocity information; “H” is the host galaxy.

SDSS ID (DR7)	Other ID	K11 ID	RA (J2000)	Dec (J2000)	APO v (km s ⁻¹)	SDSS v (km s ⁻¹)	Lit v (km s ⁻¹)	Dist (Mpc)	r (mag)	Status
	NGC4258		184.74000	47.30400	451		456	7.60 ^c	10.10	H
588017111295918190	SDSS J121551.55+473016.8		183.96482	47.50469		654	650		16.74	Y
588017109685633092	NGC 4288		185.15895	46.29180	527	522	528	8.05 ^b	13.18	Y
588298663036846207	SDSS J121933.21+472705.2	S8	184.88838	47.45147		786	788	7.05 ^d	17.13	Y
588298663036715072	NGC 4248	S4	184.45768	47.40920	482		492	7.40 ^b	13.08	Y
588017110759243996		S7	184.78782	47.08978		136		7.24 ^b	16.09	Y
588298662499844277	SDSS J121811.04+465501.2	S5	184.54613	46.91686	390	387	480	6.54 ^b	16.59	Y
588017109685174480			183.66661	46.35330		583			17.99	Y
588017111832920080	2MASX J12173195+4759420		184.38344	47.99523		684	705	702	15.30	Y
588298664110653634	UGC 07392	S10	185.07288	48.13766	819	805	805		15.82	M
588017111295590521	SDSS J121134.99+473927.1		182.89582	47.65755	749		755		17.30	M
588017605758222436			185.31344	45.81202	439	444		7.06 ^b	14.72	M
588017627228930090	NGC 4242		184.37573	45.61930		528	514	7.90 ^b	13.32	M
588017627765997621	UGC 07391		185.06768	45.90840	751	619	620		15.81	M
588297863121272860	NGC 4144		182.49338	46.45740	261	263	273	7.24 ^b	12.14	M
588298663036846358			184.86350	47.31255				7.05 ^d	18.32	M
588298663573782593	UGC 07401	S13	185.20176	47.82592	759	757	770		15.78	M
588298663573717422	[KK98] 132	S6	184.77705	47.73024					20.40	X
588017110759113395		P5	184.15612	47.15199					22.38	X
588017110222504639		S14	185.22911	46.83067					18.17	X
588298662499779244		P4	184.25990	46.90557					20.62	X
588298663036912678		S11	185.12007	47.49025					23.38	X
588298663037239998			186.27526	47.31420	N/A				18.44	X
588298662499779283		P3	184.27664	46.90220					21.19	X
588298663573651859		P1	184.57699	47.80259					23.92	X
588017110759309970		S9	184.90003	47.09313					18.64	X
588017111296508012		S16	185.94219	47.65887					19.20	X
588017110759637262			186.04768	47.12249	N/A				17.77	X
588297864195342828		S1	183.52064	47.43611					18.98	X
588298662500041067		S12	185.16674	47.00117	N/A				23.99	X
588298661962974110	[KKH2011] P2	P2	184.52705	46.48063					22.25	X
588017111295721701			183.29386	47.68492	>10,000				18.36	N
588017112369857019			184.70784	48.52569	13007				18.13	N
588017112370380911	UGCA 281		186.56543	48.49401		364	289	5.63 ^b	15.28	N
588298662499844430			184.49752	46.94287		1149			17.98	N
588017606294700206	UGC 07301		184.17534	46.07877		709	698	21.50 ^a	14.69	N
588017606294831288			184.65277	46.08295	>10,000				18.33	N
588017110222176377	MCG +08-22-086		184.00925	46.73285	1073		1065		15.37	N
588017627765866639	SDSS J121840.14+455434.9		184.66725	45.90971		1045	1062		16.33	N
588298663574110513			186.15665	47.70873	>10,000				17.95	N
588298664110260438			183.81594	48.21531	>10,000				18.51	N
588297863658340527	MCG +08-22-083		182.98213	46.98181		972	975		16.00	N
588298661963694280			186.86392	46.55062	>10,000				18.18	N
588298661963694346			186.86750	46.54675	>10,000				18.65	N
588017605758550042			186.39419	45.68523	717	712		14.40 ^a	12.18	N
588298662500302850	NGC 4346	S15	185.86649	46.99378	780		778	15.70 ^a	11.41	N
588298664110325782	NGC 4218	S2	183.94336	48.13084	685	796	738	21.10 ^a	13.47	N
588298663573454909	NGC 4220	S3	184.04879	47.88324	887		922	17.90 ^a	11.58	N

NGC 4258 Satellites

^a NED

^b Karachentsev et al. (2013)

^c Humphreys et al. (2013)

^d Munshi & Macri (2007)

5. ACKNOWLEDGEMENTS

The authors would like to thank L. Macri and F. Munshi for distance measurements to SDSS IDs 207 and 358. They would also like to thank M. Mateo and M. Valluri for many useful conversations and feedback, as well as E. Bell and C. Slater for the insight into distance measures and the reference to the Karachentsev et al. (2013) catalog of Local Volume galaxies. The authors also thank the anonymous referee for the useful comments. SL acknowledges funding from the Michigan Society of Fellows and thanks the ever cromulent S. Garner.

This work was based in part on observations obtained with the Apache Point Observatory 3.5-meter telescope, which is owned and operated by the Astrophysical Research Consortium. We thank the APO observing specialists for their help in executing these observations.

GANDALF was developed by the SAURON team and is available from the SAURON website (www.strw.leidenuniv.nl/sauron). See also Sarzi et al. (2006) for details.

This research made use of the NASA/IPAC Extragalactic Database (NED), which is operated by the Jet Propulsion Laboratory, California Institute of Technology, under contract with the National Aeronautics and Space Administration.

Funding for SDSS-III has been provided by the Alfred P. Sloan Foundation, the Participating Institutions, the National Science Foundation, and the U.S. Department of Energy Office of Science. The SDSS-III web site is <http://www.sdss3.org/>.

SDSS-III is managed by the Astrophysical Research Consortium for the Participating Institutions of the SDSS-III Collaboration including the University of Arizona, the Brazilian Participation Group, Brookhaven National Laboratory, University of Cambridge, Carnegie Mellon University, University of Florida, the French Participation Group, the German Participation Group, Harvard University, the Instituto de Astrofísica de Canarias, the Michigan State/Notre Dame/JINA Participation Group, Johns Hopkins University, Lawrence Berkeley National Laboratory, Max Planck Institute for Astrophysics, Max Planck Institute for Extraterrestrial Physics, New Mexico State University, New York University, Ohio State University, Pennsylvania State University, University of Portsmouth, Princeton University, the Spanish Participation Group, University of Tokyo, University of Utah, Vanderbilt University, University of Virginia, University of Washington, and Yale University.

REFERENCES

- Bailin, J., Power, C., Norberg, P., Zaritsky, D., & Gibson, B. K. 2007, *ArXiv e-prints*, 706
- Barber, C., Starkenburg, E., Navarro, J., McConnachie, A., & Fattahi, A. 2013, *ArXiv e-prints*
- Boylan-Kolchin, M., Bullock, J. S., Sohn, S. T., Besla, G., & van der Marel, R. P. 2013, *ApJ*, 768, 140
- Burkert, A. 1995, *ApJ*, 447, L25
- Cappellari, M., & Emsellem, E. 2004, *PASP*, 116, 138
- Caproni, A., Abraham, Z., Livio, M., & Mosquera Cuesta, H. J. 2007, *MNRAS*, 379, 135
- Carrasco, E. R., Mendes de Oliveira, C., & Infante, L. 2006, *AJ*, 132, 1796
- Chiboucas, K., Jacobs, B. A., Tully, R. B., & Karachentsev, I. D. 2013, *AJ*, 146, 126
- Chonis, T. S., & Gaskell, C. M. 2008, *AJ*, 135, 264
- Conn, A. R., Lewis, G. F., Iбата, R. A., Parker, Q. A., Zucker, D. B., McConnachie, A. W., Martin, N. F., Valls-Gabaud, D., Tanvir, N., Irwin, M. J., Ferguson, A. M. N., & Chapman, S. C. 2013, *ArXiv e-prints*
- de Vaucouleurs, G., de Vaucouleurs, A., Corwin, Jr., H. G., Buta, R. J., Paturel, G., & Fouqué, P. 1991, *Third Reference Catalogue of Bright Galaxies. Volume I: Explanations and references. Volume II: Data for galaxies between 0^h and 12^h. Volume III: Data for galaxies between 12^h and 24^h.*
- Erickson, L. K., Gottesman, S. T., & Hunter, Jr., J. H. 1999, *ApJ*, 515, 153
- Geha, M., Blanton, M. R., Yan, R., & Tinker, J. L. 2012, *ApJ*, 757, 85
- Hartwick, F. D. A. 2000, *AJ*, 119, 2248
- Holmberg, E. 1969, *Arkiv for Astronomi*, 5, 305
- Humphreys, E. M. L., Reid, M. J., Greenhill, L. J., Moran, J. M., & Argon, A. L. 2008, *ApJ*, 672, 800
- Humphreys, E. M. L., Reid, M. J., Moran, J. M., Greenhill, L. J., & Argon, A. L. 2013, *ApJ*, 775, 13
- Iбата, R. A., Lewis, G. F., Conn, A. R., Irwin, M. J., McConnachie, A. W., Chapman, S. C., Collins, M. L., Fardal, M., Ferguson, A. M. N., Iбата, N. G., Mackey, A. D., Martin, N. F., Navarro, J., Rich, R. M., Valls-Gabaud, D., & Widrow, L. M. 2013, *Nature*, 493, 62
- Karachentsev, I. D., Makarov, D. I., & Kaisina, E. I. 2013, *AJ*, 145, 101
- Kim, E., Kim, M., Hwang, N., Lee, M. G., Chun, M.-Y., & Ann, H. B. 2011, *MNRAS*, 412, 1881
- Kroupa, P., Theis, C., & Boily, C. M. 2005, *A&A*, 431, 517
- Ludwig, J., Pasquali, A., Grebel, E. K., & Gallagher, III, J. S. 2012, *AJ*, 144, 190
- Martin, R. G. 2008, *MNRAS*, 387, 830
- Mateo, M. 2008, *The Messenger*, 134, 3
- Mateo, M. L. 1998, *ARA&A*, 36, 435
- McMillan, P. J. 2011, *MNRAS*, 414, 2446
- Munshi, F., & Macri, L. 2007, in *Bulletin of the American Astronomical Society*, Vol. 39, American Astronomical Society Meeting Abstracts, 827
- Navarro, J. F., Frenk, C. S., & White, S. D. M. 1996, *ApJ*, 462, 563
- Nesti, F., & Salucci, P. 2013, *JCAP*, 7, 16
- Newman, J. A., Ferrarese, L., Stetson, P. B., Maoz, E., Zepf, S. E., Davis, M., Freedman, W. L., & Madore, B. F. 2001, *ApJ*, 553, 562
- Prada, F., Vitvitska, M., Klypin, A., Holtzman, J. A., Schlegel, D. J., Grebel, E. K., Rix, H.-W., Brinkmann, J., McKay, T. A., & Csabai, I. 2003, *ApJ*, 598, 260
- Sarzi, M., Falcón-Barroso, J., Davies, R. L., Bacon, R., Bureau, M., Cappellari, M., de Zeeuw, P. T., Emsellem, E., Fathi, K., Krajnović, D., Kuntschner, H., McDermid, R. M., & Peletier, R. F. 2006, *MNRAS*, 366, 1151
- van Albada, G. D. 1977, *A&A*, 61, 297
- Vazdekis, A., Sánchez-Blázquez, P., Falcón-Barroso, J., Cenarro, A. J., Beasley, M. A., Cardiel, N., Gorgas, J., & Peletier, R. F. 2010, *MNRAS*, 404, 1639
- Watkins, L. L., Evans, N. W., & An, J. H. 2010, *MNRAS*, 406, 264
- Zaritsky, D. 1992, *ApJ*, 400, 74
- Zaritsky, D., Smith, R., Frenk, C., & White, S. D. M. 1993, *ApJ*, 405, 464
- Zentner, A. R., Kravtsov, A. V., Gnedin, O. Y., & Klypin, A. A. 2005, *ApJ*, 629, 219